Spring 2023

A Real-Time Microwave Camera Using Zero-Bias Diode Detector

Liang Liu
Missouri University of Science and Technology

Department:

A REAL-TIME MICROWAVE CAMERA USING ZERO-BIAS DIODE DETECTOR

by

LIANG LIU

A THESIS

Presented to the Graduate Faculty of the

MISSOURI UNIVERSITY OF SCIENCE AND TECHNOLOGY

In Partial Fulfillment of the Requirements for the Degree

MASTER OF SCIENCE

in

ELECTRICAL ENGINEERING

2022

Approved by:

Dr. Victor Khikevich, Advisor
Dr. DongHyun Kim
Dr. Chulsoon Hwang

ABSTRACT

This thesis presents the design of a microwave camera that utilizes a two-dimensional array of elliptical slot antennas and diode detectors to quickly and accurately locate radiation sources. Unlike traditional scanning techniques like ESM and holography, which rely on mechanical scanning, require a long measurement time, and are prone to mechanical errors, the microwave camera operates quickly and efficiently by using electronic switching to access the output of each detector. This results in a more precise and efficient means of locating radiation sources.

ACKNOWLEDGMENTS

I would like to express my gratitude to several people who have supported and helped me throughout my master's program. First and foremost, my advisor, Dr. Khilkevich Victor, provided invaluable advice, support, and encouragement that helped me overcome many challenges. I also want to thank Dr. DongHyun Kim and Dr. Chulsoon Hwang for their contributions to my research. I am grateful to my parents and friends for their encouragement and support throughout my studies. Lastly, I would like to extend my thanks to all members of the Electromagnetic Compatibility Laboratory at Missouri University of Science and Technology for their help in completing my research smoothly.

TABLE OF CONTENTS

Page

ABSTRACT iii

ACKNOWLEDGMENTS iv

LIST OF ILLUSTRATIONS vi

SECTION

1. INTRODUCTION 1
2. ELLIPTICAL SLOT ANTENNA 3
   - 2.1. INTRODUCTION 3
   - 2.2. ANTENNA CHARACTERIZATION 5
     - 2.2.1. Full Wave Simulation Analysis 5
     - 2.2.2. Antenna Parameter Measurement 7
3. DIODE DETECTOR CIRCUIT 12
   - 3.1. INTRODUCTION 12
   - 3.2. DETECTOR CIRCUIT CHARACTERIZATION 13
   - 3.3. DETECTOR CIRCUIT WITH ELLIPTICAL SLOT ANTENNA 16
4. ANTENNA ARRAY 21
   - 4.1. ARCHITECTURE OF THE PROPOSED CAMERA SENSOR 21
   - 4.2. ELECTRONIC COMPONENTS OF THE SENSOR 23
   - 4.3. CHARACTERIZATION OF THE ANTENNA ARRAY (NO AMPLIFIER) 24
   - 4.4. ACHIEVABLE SENSITIVITY WITH THE AMPPLIFIER 26
   - 4.5. FRAME RATE 27
5. CONCLUSIONS 30

REFERENCES 31

VITA 32

LIST OF ILLUSTRATIONS

Figure Page

2.1. Elliptical Slot Antenna Prototype 4

2.2. Simplified Antenna Model in CST 5

2.3. Simulated S11 of The Elliptical Antenna Model 6

2.4. Simulated Antenna Gain 7

2.5. Simulated Radiation Pattern of The Antenna 8

2.6. Antenna Characterization Setup 8

2.7. Measured S11 of The Elliptical Slot Antenna 9

2.8. Horn Antenna Gain 11

3.1. Diode Package and Schematic 12

3.2. BAT15-04W Characteristics 13

3.3. Detector Circuit Schematic 13

3.4. Prototype of Detector Circuit 14

3.5. Diode Characterization Setup 14

3.6. Attenuation Measurement Setup 15

3.7. S21 of The Attenuators 16

3.8. Detecetor Output Voltage VS Input Power at 10 GHz 17

3.9. Detector Output Voltage VS Frequency 17

3.10. Antenna-Detector Characterization Setup 18

3.11. Detector Output Voltage VS E-field Strength 19

3.12. Detector Output Voltage vs Frequency 20

4.1. Antenna Element Schematic 21

4.2. Architecture of The Camera Sensor 22

4.3. SparkFun Multiplexer Breakout - 8 Channel (74HC4051) 23

4.4. Arduino Mega 2560 24
4.5. Proto Amplifier Module AD 620 25
4.6. Measurement Setup for Antenna Array 25
4.7. Maximum Voltage of Antenna Array vs E Field Strength 26
4.8. Image Produced by The Sensor in The Setup in Figure 4.6 27
4.9. The Sensitivity of Camera Sensor with The Amplifer 28
4.10. Frame Rate Measurement Setup 28
4.11. Camera Sensor Output Voltage Waveform 29

1. INTRODUCTION

The Emission Source Microscopy (ESM) technique [1] is employed for imaging Electromagnetic Interference (EMI) sources, aiding engineers in identifying the origin of the far-field radiation. The traditional ESM requires mechanical scanning to gather electrical field data across a 2D plane, which can take significant time- up to several hours. This work introduces a real-time microwave camera, capable of obtaining EMI source images much faster than traditional mechanical scanning methods. The proposed camera utilizes a diode detector circuit, which offers relatively high sensitivity, enabling measurement of EMI sources with low power levels.

Previous studies in this field are discussed in [2]. This paper presents a novel, portable real-time microwave camera. The design of the camera begins by outlining the elliptical slot antenna, which serves as the element in the antenna array. The antenna is simulated through full-wave analysis and its performance is verified through measurement. Following this, a diode detector circuit is introduced, and its sensitivity is evaluated through experimentation.

The second portion of the paper introduces the antenna array architecture and demonstrates its ability to detect Electromagnetic Interference (EMI) sources.The performance of the array is analyzed through various measurements.

The paper [1] presents the use of emission source microscopy (ESM) to localize Electromagnetic Interference (EMI) sources. In ESM, the amplitude and phase of the RF signal are measured, and an image is recovered mathematically. The study in the paper shows that while ESM is capable of localizing EMI sources, it requires scanning equipment and an expensive receiver (VNA or oscilloscope).

In contrast, my thesis proposes a design that only measures DC signal from diode detector, eliminating the need for RF switching. However, this design requires an additional imaging system, such as a lens or a holographic setup, to recover the image. The advantage of the proposed design is that it doesn't require an expensive and complex receiver, making it more accessible and more cost-effective.

The proposed design has some limitations, including a lack of frequency selectivity and relatively low sensitivity compared to traditional instruments such as a Vector Network Analyzer (VNA), Spectrum Analyzer (SA), or oscilloscope, which were used in the design presented in the paper[2]. As a result, a strong dedicated source is required to be captured by diode detector circuit.

However, the proposed design still provides some potential applications, including the visualization of EMI from passive structures like Printed Circuit Boards (PCBs) in real-time. The ability to visualize EMI sources in real-time provides valuable information for improving electromagnetic compatibility, especially for large and complex systems. Despite its limitations, the proposed design provides a simple and accessible alternative for EMI source localization.

2. ELLIPTICAL SLOT ANTENNA

This section of the thesis focuses on the introduction and evaluation of an elliptical slot antenna. It provides a brief overview of the antenna and then uses full-wave simulations to assess its characteristics. The simulation results are then validated through various measurements. The goal of this section is to study the behavior of the elliptical slot antenna and determine its suitability for use in the proposed microwave camera design. Through simulation and experimentation, the author aims to gain a comprehensive understanding of the antenna's performance and use this information to inform the design of the microwave camera.

2.1. INTRODUCTION

Slot antenna is widely used in different areas, including PCB technology. It is popular in printed circuit boards due to low profile, light weight, and wide bandwidth. There are many ways to feed slot antenna.

In this work, an elliptical slot antenna with coplanar waveguide is designed as the receiver of the real-time camera sensor. The antenna prototype is shown in Figure 2.1

Figure 2.1 present a prototype of an elliptical slot antenna with coplanar waveguide. An SMA connector is attached to the antenna output. Via stitching is used in the antenna design to connect the top ground layer to the bottom layer. The impedance of waveguide is well tuned to 50 Ohm.

A simplified model (Figure 2.2) is used to characterize the performance of the antenna.

Before the PCB prototype of the elliptical antenna is fabricated by the PCB manufacturer, the antenna model is simulated in CST, a high-performance 3D EM analysis software using FIT (finite integration technique) algorithm. The dimension of the antenna model is described in Figure 2.2. Compared with the antenna prototype, the antenna model in CST

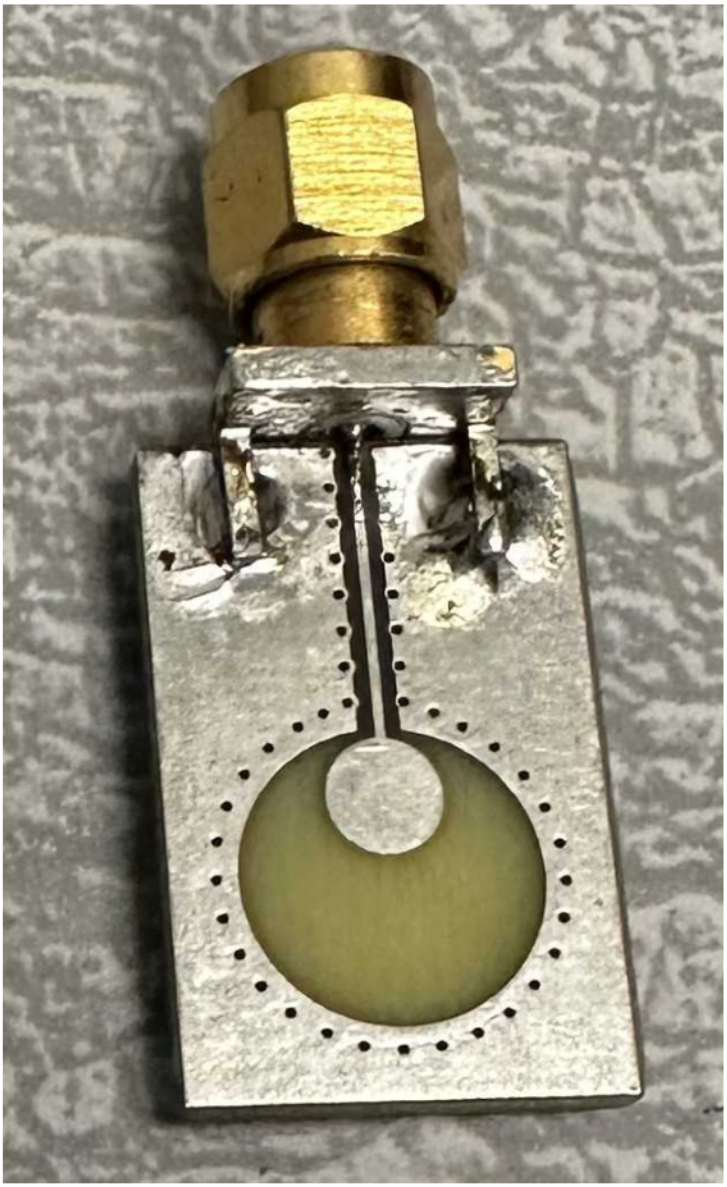

Figure 2.1. Elliptical Slot Antenna Prototype

is simplified by removing the coplanar waveguide and via stitching to reduce the simulation time. Removing the coplanar waveguide doesn't impact the accuracy of the simulation because the length of the wavelength is very small (1-2 cm) and it provides small loss for the signal received by the elliptical antenna.

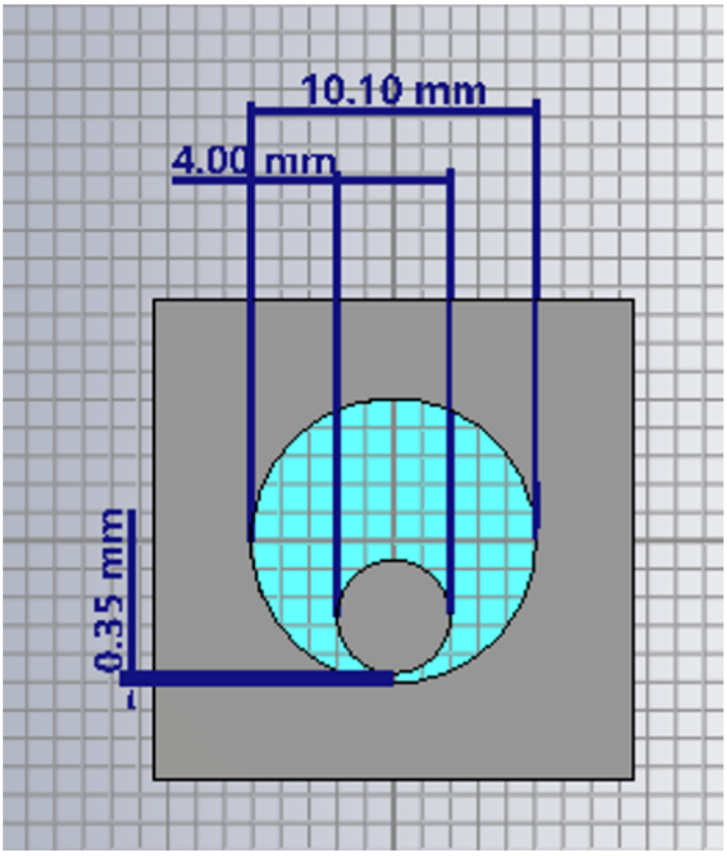

Figure 2.2. Simplified Antenna Model in CST

2.2. ANTENNA CHARACTERIZATION

In this section, simluation and measurement are done to characterize the performance of antenna, which is crucial for the further study about antenna array.

2.2.1. Full Wave Simulation Analysis. Figure 2.2 shows a simplified slot antenna model in CST. A discrete port is placed at the gap between the central elliptical conductor and the top ground plane. The model is surrounded by vacuum and the boundary condition is open. The simulation frequency is set from 1GHz to 25 GHz. To evaluate the antenna performance, the reflection coefficient S11, antenna gain at the direction perpendicular to the board and antenna pattern were calculated.

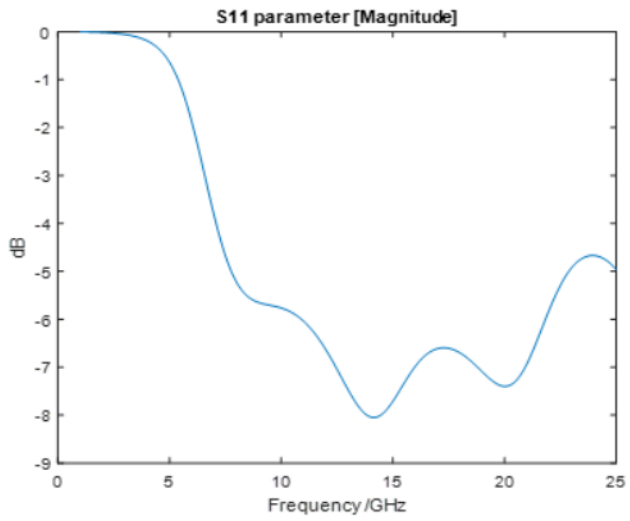

Figure 2.3. Simulated S11 of The Elliptical Antenna Model

Optimizing the antenna design to achieve a low value of S11 is crucial to ensure efficient power transfer from slot antenna to detector circuit and to minimize the power loss due to reflections. A high S11 value can result in decreased antenna efficiency, lower radiation efficiency, and reduced gain. .

In antenna design, one of the most important parameters is S11. As can be seen from Figure 2.3, S11 of the antenna is below -5 dB from 8 GHz to 23 GHz. When S11 is below -5dB, it means that less than 3.2% of the power is being reflected back to the source, which indicates that the antenna is efficiently transferring power to the 50 ohm load. In this frequency range, the antenna has a good capacity to receive the RF signal. If we define the bandwidth is the frequency range where S11 is below -5 dB, the bandwidth of the antenna is 15 GHz.

Another useful merit describing the performance of an antenna is the gain. It is a measure to show the efficiency of the antenna as well as its directional capabilities. Antenna Gain describes how much power is transmitted in the direction of peak radiation compared to that of an isotropic source[3]. In Figure 2.4, the antenna gain remains around 5 dB from

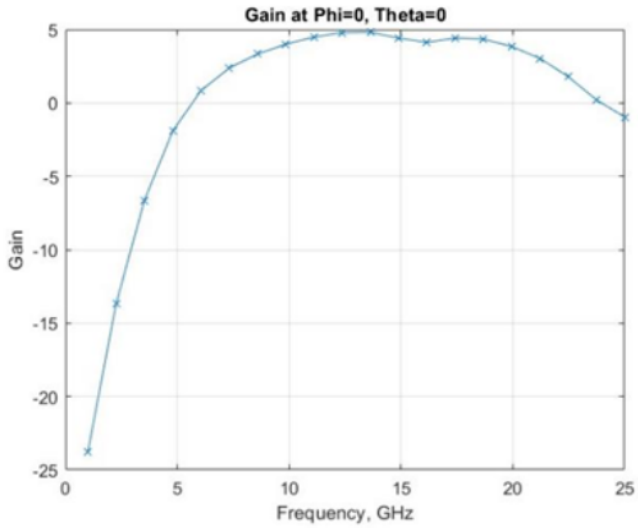

Figure 2.4. Simulated Antenna Gain

10 GHz to 20 GHz in the direction perpendicular to the top layer of the PCB prototype.The antenna exhibits peak gain between 10 GHz and 20 GHz, which demonstrates that the microwave camera is optimized to operate effectively within this frequency range.

The radiation pattern of the antenna refers to the directional distribution of electromagnetic energy emitted or received by an antenna. It is a graphical representation of how the radiated or received energy is distributed in space. From Figure 2.5 it can be seen that, when the elevation angle theta is equal to 0 or 180 degrees and the azimuth angle phi is equal to 90 degree, the antenna has the maximum amplitude of E field in those directions. When the theta is equal to 90 or 270 degree, the antenna has the minimum amplitude of E field. EMI source should be place in the direction(Theta = 0 degree or 180) to achieve the maximum antenna efficiency.

2.2.2. Antenna Parameter Measurement. To verify the performance of antenna, a measurement setup is assembled to characterize several merits of elliptical antenna (Figure 2.6).

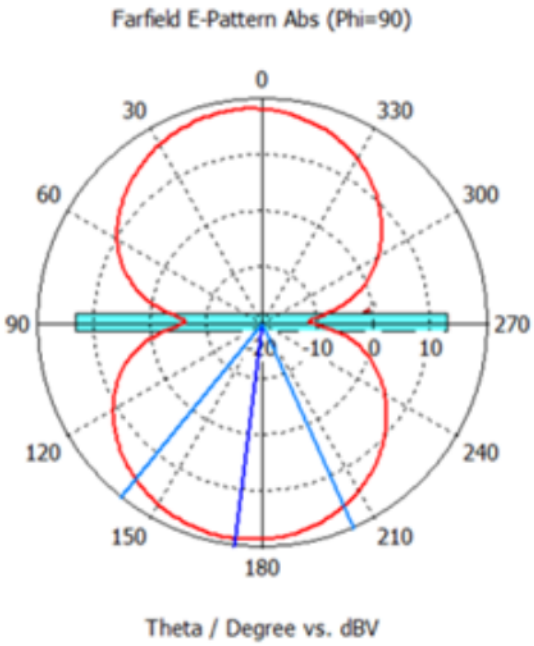

Figure 2.5. Simulated Radiation Pattern of The Antenna

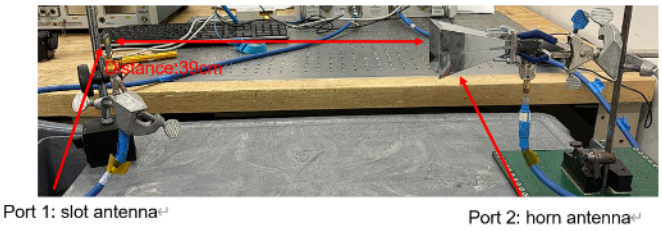

Figure 2.6. Antenna Characterization Setup

The VNA (Vector Network Analyzer) is used to measure the S-parameters between a horn antenna and an elliptical antenna in order to characterize the performance of the antenna. In order to eliminate the effect of the cables, the VNA is calibrated using an E-cal kit. The distance between two antennas is 39 cm. The S11 of the slot antenna can be directly acquired by VNA. The S11 results is shown in Figure 2.7.

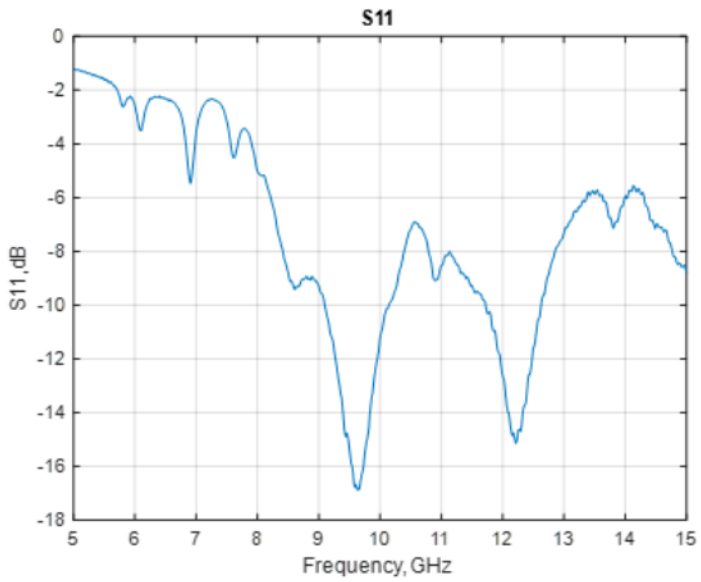

Figure 2.7. Measured S11 of The Elliptical Slot Antenna

As follows from Figure 2.7, there are two local minima at 9.8 GHz and 12.2 GHz respectively. At these frequency points, S11 is below -14 dB. In the simulation, S11 is around -7 dB from 13 GHz to 20 GHz. However, based on the measurement results, the antenna has better match over the frequency range compared with simulation results.

To calculate the gain of elliptical slot antenna, Friis transmission equation is used. The Friis equation is used to calculate the received power from the transmitted power between two antennas separated by a certain distance.

The equations is

$$\frac{P_r}{P_t} = G_t G_r (\frac{\lambda}{4\pi d})^2 \tag{2.1}$$

where P_r the power received by the receiving antenna. P_t is the power fed into the transmitting antenna input terminals. G_t is the gain of the transmitting antenna. G_r is the gain of the receiving antenna. λ is the wavelength.and d is the distance separating the antennas.

Ohm's law relates the power dissipated on the resistor R and the voltage V applied to it:

$$P = \frac{V^2}{R} \tag{2.2}$$

In turn the transmission coefficient is defined as

$$S21 = \frac{V_2^-}{V_1^+} \tag{2.3}$$

where V_2^- is the amplitude of the outgoing wave in port 2 (receiving antenna), and V_1^+ is the amplitude of the incident wave in port 1 (transmitting antenna).

The transmitted power is related to the incident wave on port 1 as

$$P_t = \frac{|V_1^+|^2}{R} \tag{2.4}$$

and the received power to the amplitude of the outgoing wave at port 2 as

$$P_r = \frac{|V_2^-|^2}{R} \tag{2.5}$$

where R is the reference impedance.

By taking the ratio of the transmitted and received power one can find:

$$\frac{P_t}{P_r} = |S21|^2 \tag{2.6}$$

Taking this into account the equation of the gain of the slot antenna can be derived:

$$G_{slot} = |S21|^2 \cdot \frac{1}{G_{horn}} \cdot (\frac{4\pi d}{\lambda})^2 \tag{2.7}$$

Where G_{Horn} is the gain of the horn antenna.

The gain of the horn antenna is known in the frequency range from 8 to 12 GHz (Figure 2.8).

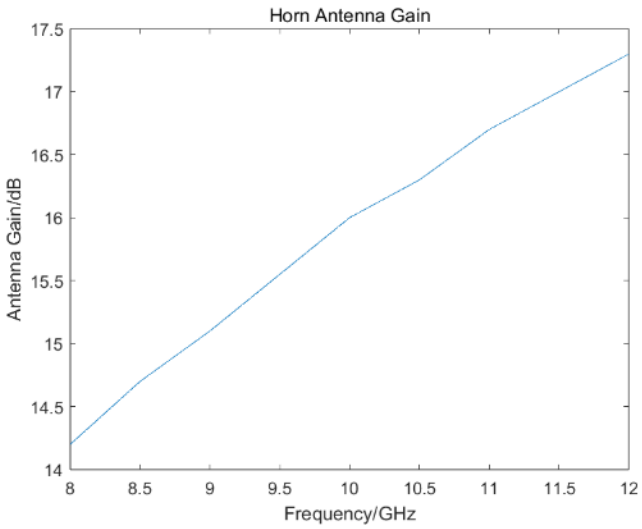

Figure 2.8. Horn Antenna Gain

The gain of elliptical slot antenna is also calculated in that frequency range using (2.7).

3. DIODE DETECTOR CIRCUIT

This section covers the discussion of the diode detector circuit, including characterization of the diode detectors. Several measurements are conducted to verify the performance of the diode detector.

3.1. INTRODUCTION

The design utilizes the BAT15-04W Schottky diode from Infineon, which is well-suited for RF applications as it offers a low barrier height, low forward voltage, and low junction capacitance. The component, including its port mapping and internal structure, is presented in Figure 3.1.

The elctrical characteristics of the diode pair is obtained from the datasheet (Figure 3.2)

The proposed detector design follows the Infineon application note [4] (Figure 3.3).

Figure 3.4 depicts the detector circuit prototype, which incorporates two SMA connectors on the board. The circuit comprises of a diode pair, BAT15-04W, represented by D1 in the schematic in Figure 3.3. Additionally, the circuit includes two capacitors, C1 and

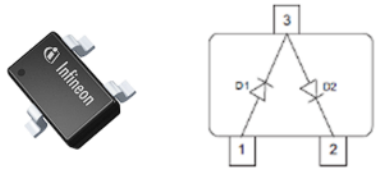

Figure 3.1. Diode Package and Schematic

Parameter	Values			Unit	Note or test condition
	Min.	Typ.	Max.		
Breakdown voltage	4	-	-	V	$I_R = 100\,\mu A$
Reverse current	-	-	5	μA	$V_R = 1V$
Forward voltage	0.16	0.25	0.32	V	$I_F = 1\ mA$
	0.25	0.35	0.41		$I_F = 10\ mA$
Forward voltage matching	-	-	20	mV	$I_F = 10$ mA
Differential forward resistance	-	5.8	-	ohm	$I_F = 10$ mA / 50 mA
Capacitance	-	0.3	0.35	pF	$V_R = 0$ V, $f = 1$ MHz
inductance	-	1.4	-	nH	

Figure 3.2. BAT15-04W Characteristics

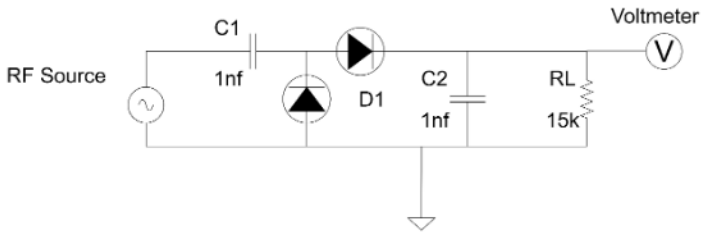

Figure 3.3. Detector Circuit Schematic

C2, which are recommended in the application note. The load resistance of the circuit is denoted by RL. C1 block DC signal from RF source. To ensure low ohmic capacitive reactance down to 6 GHz, a 1 nF bypass capacitor (C2) was selected. The frequency range of the detector circuit is determined by the diode. The detection sensitivity of the circuit relies on RL.

3.2. DETECTOR CIRCUIT CHARACTERIZATION

To characterize the performance the following setup is used (Figure 3.5).

Figure 3.4. Prototype of Detector Circuit

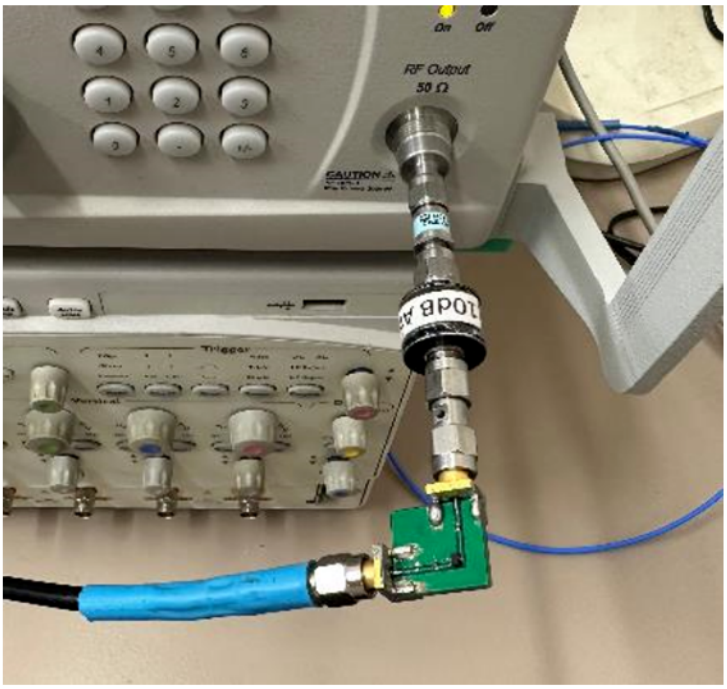

Figure 3.5. Diode Characterization Setup

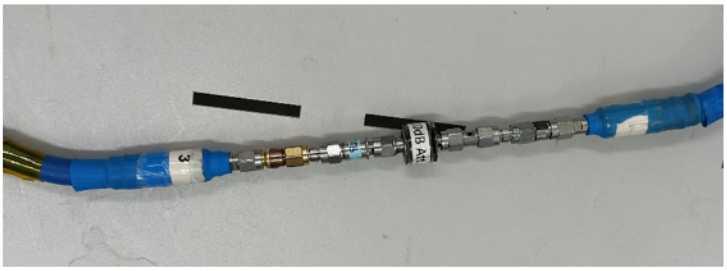

Figure 3.6. Attenuation Measurement Setup

In the setup, Anritsu MG3692C generator is used to generate RF signals. Multiple attenuators are cascaded to reduce the input power of the detector circuit, as the RF generator can only output a minimum power of -20 dBm. The attenuation offered by the cascaded attenuators is frequency-dependent across a range of frequencies. Therefore, to accurately determine the input power of the detector circuit, it is necessary to evaluate frequency-dependent attenuation across frequency range. The setup illustrated in Figure 3.6is employed to characterize the attenuator.

Figure 3.7 displays the S21 of the attenuators. The measurement of S21 is carried out using a VNA (Vector Network Analyzer).

The S21 values of the attenuators are utilized to determine the precise input power of the detector circuit. To evaluate the performance of the detector circuit, two measurements are performed. The first measurement involves sweeping the input power of the detector board at a constant frequency (10 GHz). The outcome of this measurement is depicted in Figure 3.8

In Figure 3.8, at the initial stages of the curve, the output voltage of the detector circuit exhibits slight fluctuations at very low input power levels. The small variation in the output voltage at the beginning suggests that the detector circuit has not yet received

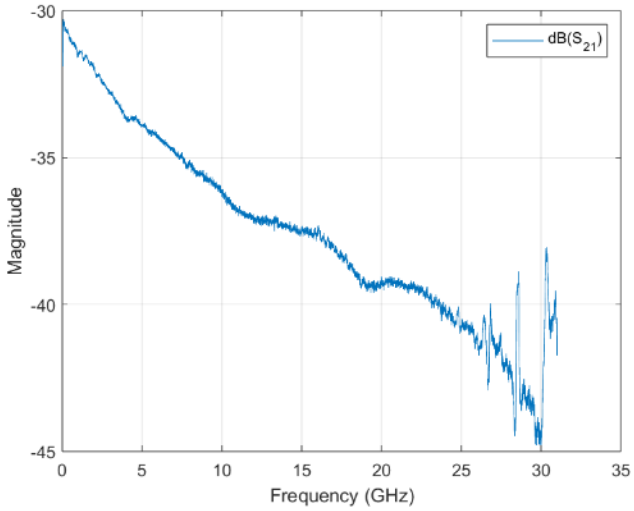

Figure 3.7. S21 of The Attenuators

sufficient power, and the voltage measured at this level is most likely due to random noise. As the input power increases, a linear relationship between the input power and the output voltage emerges, starting from an input power level of -53 dBm (minimal detectable power).

The second measurement involves measuring the output voltage of the detector circuit across a range of frequencies while maintaining a constant input power level (-35 dBm). The outcome of this measurement is illustrated in Figure 3.9.

The output voltage varies across the frequency range with the peaks observed at 5 GHz and 10.5 GHz.

3.3. DETECTOR CIRCUIT WITH ELLIPTICAL SLOT ANTENNA

In the next experiment the elliptical antenna board was connected to the detector board in order to simulate the performance of a single element in the antenna array. However, it should be noted that the results obtained from this setup may not be identical to those

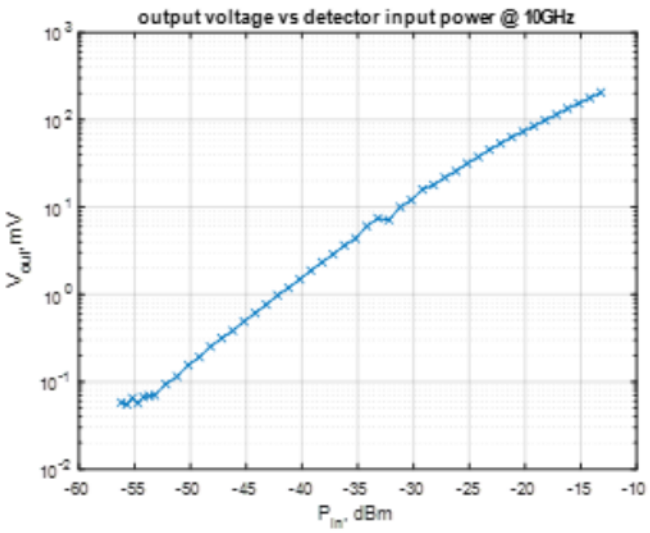

Figure 3.8. Detecetor Output Voltage VS Input Power at 10 GHz

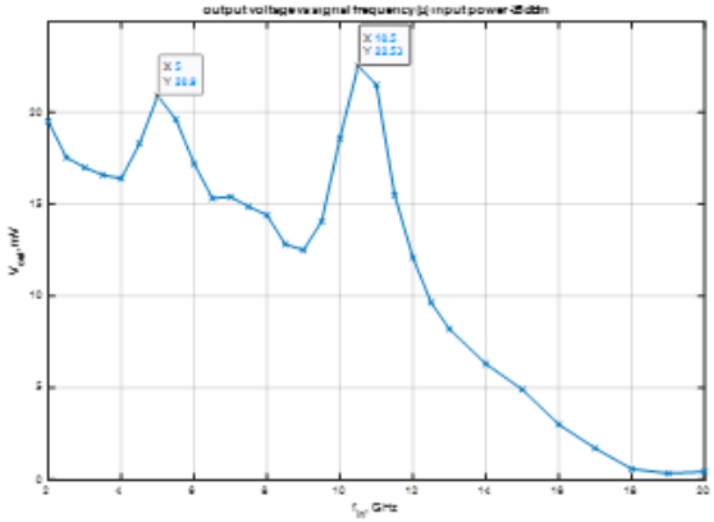

Figure 3.9. Detector Output Voltage VS Frequency

observed when using an actual antenna array, as the interference between the elements in the array is not taken into account. Figure 3.10 illustrates the measurement setup used in this experiment.

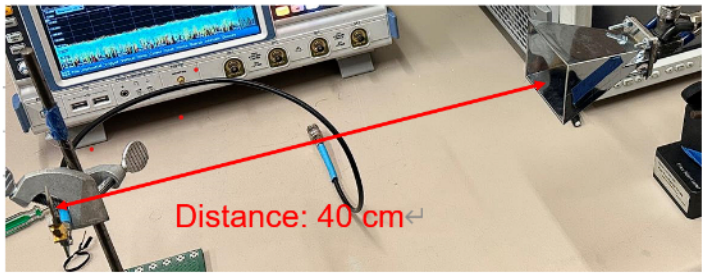

Figure 3.10. Antenna-Detector Characterization Setup

The RF signal is emitted by the horn antenna is received by the elliptical slot antenna, and the output voltage of the detector board is measured by an oscilloscope. The distance between the antennas is 40 cm, and two measurements are performed to assess the performance of array element. These measurements are similar to those conducted for the detector circuit, but in this case, the input power for the detector circuit is not applied directly from the RF generator. Instead, it is received by the slot antennas, and the strength of the applied E-field to the antenna is used as a representation of the power received by slot antenna. To calculate the strength, the following equation is used [3]:

$$E = \frac{\sqrt{30 P_{antenna} G}}{d} \tag{3.1}$$

Here $P_{antenna}$ is the power applied to horn antenna, G is the gain of the horn antenna, and d is the distance between the antennas.

Additionally, the relation between the output power of RF generator and the power received by the elliptical slot antenna is

$$P_{antenna} = P_{RF} \times |S21|^2 \tag{3.2}$$

So the final equation becomes

$$E = \frac{\sqrt{30 P_{antenna} P_{RF} |S_{21}|^2 G}}{d} \tag{3.3}$$

where E is the strength of E field at the location of the elliptical slot antenna, S_21 is the transmission coefficient between the antennas, and. P_{RF} is the output power of the RF generator.

To measure the E-field strength applied to the slot antenna, we first varied the output power of the RF generator at a fixed frequency (11.1 GHz). The output voltage of the detector board was then measured by the oscilloscope, and the results are presented in Figure 3.11. Both axes are presented on a logarithmic scale to determine the minimum electric field strength that can be detected. According to our findings, a field strength of at least 30 V/m was detectable at a distance of 40 cm at 11.1 GHz. At this field strength, the output power of the RF generator was set to -20 dBm, which represents the minimum power the generator can produce.

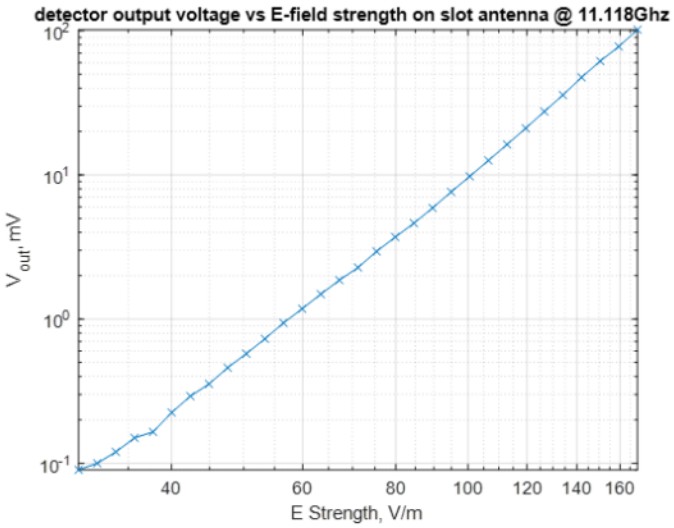

Figure 3.11. Detector Output Voltage VS E-field Strength

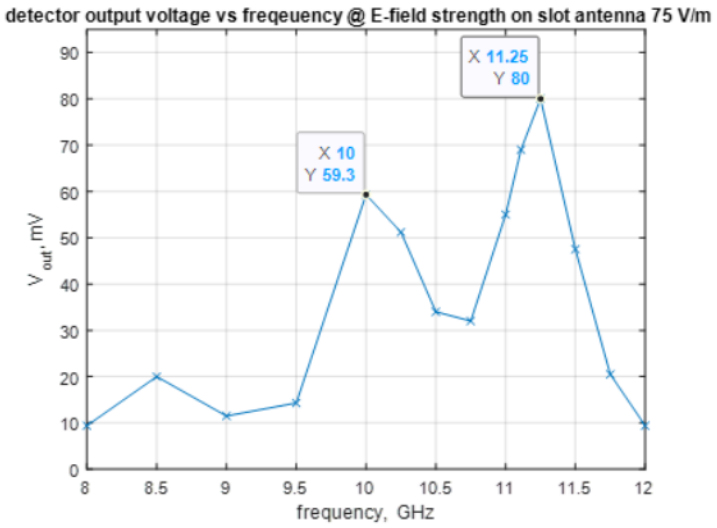

Figure 3.12. Detector Output Voltage vs Frequency

For our second measurement, we kept the E-field strength constant at 75 V/m while sweeping the frequency of the RF signal. Based on equation 3.3,the output power of the RF generator is varied across frequency range to maintain 75 V/m E-field strength at slot antenna. Figure 3.12 illustrates the results of this measurement. The plot shows two peaks, which is consistent with the measurement of a single detector board. We observed relatively high output voltages from the detector at frequencies of 10 GHz and 11.25 GHz compared to the other frequencies.

4. ANTENNA ARRAY

This section introduces the antenna array, which serves as a camera sensor for detecting unknown sources of EMI. The architecture of the antenna is explained to illustrate how it functions as a sensor. To achieve the camera sensor's overall function, various components are used, such as multiplexers, Arduino boards, and amplifier boards. Measurements are taken to assess the performance of the antenna array.

4.1. ARCHITECTURE OF THE PROPOSED CAMERA SENSOR

Figure 4.1 and Figure 4.2 illustrate the single antenna element and the camera sensor's architecture, respectively.

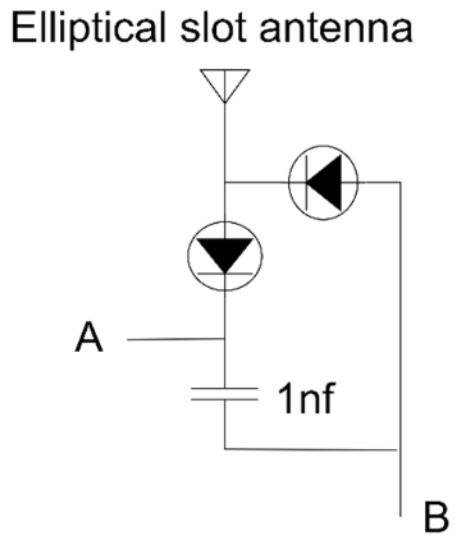

Figure 4.1. Antenna Element Schematic

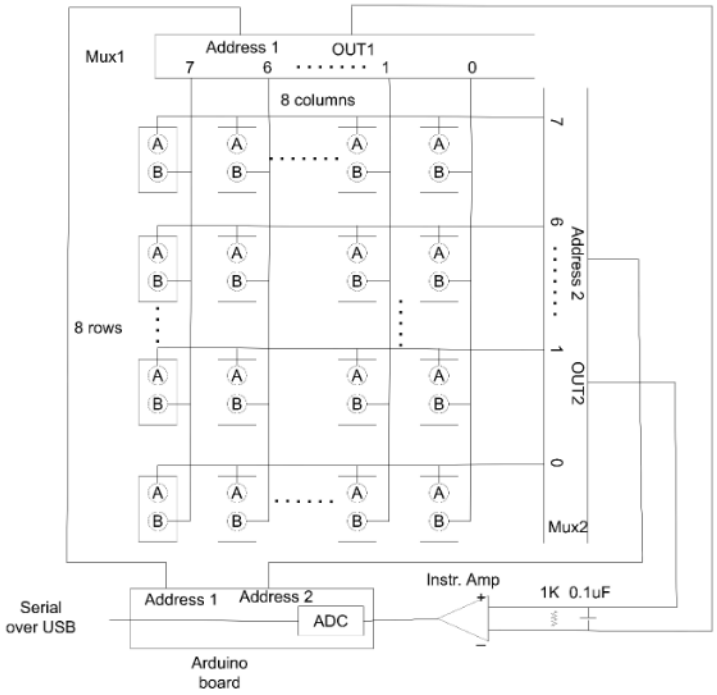

Figure 4.2. Architecture of The Camera Sensor

Figure 4.1 illustrates the diode detector analyzed in Section 3, with port ”A” as the signal, with port ”A” as the signal port and port ”B” as the ground port. A diode pair (BAT15-04W) is included in the schematic, and each antenna element corresponds to one pixel of the EMI source image. The resolution of the real-time camera is determined by the distance between the antenna elements.

In Figure 4.2, the camera sensor system of 8 rows and 8 columns of antenna elements, as well as two multiplexers, one amplifier board, and one Arduino board. Port ”A” of each antenna element is connected to the input pins of multiplexer ”2,” while port ”B” is connected to the input pins of multiplexer ”1.” The Arduino board sends out different addresses to the multiplexers, allowing the camera to address all of the antenna elements in milliseconds.

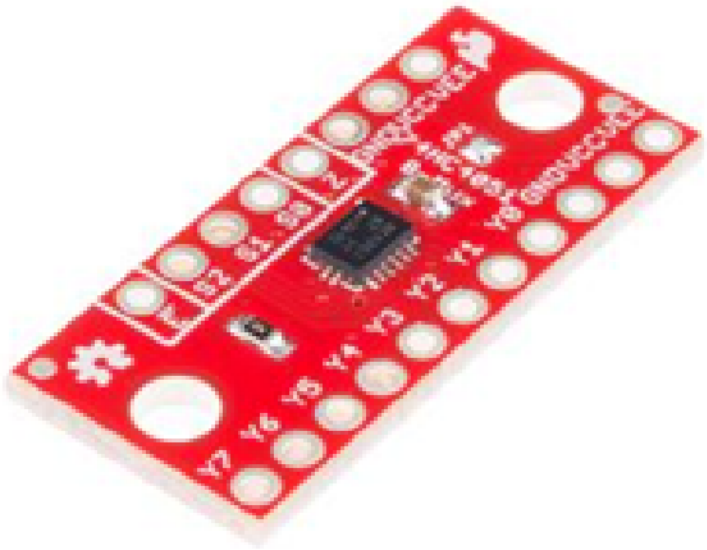

Figure 4.3. SparkFun Multiplexer Breakout - 8 Channel (74HC4051)

To suppress the switching noise created by the multiplexers, a 0.1 uF capacitor is added to the input of the instrumentation amplifier board, which is used to amplify the output voltage of each antenna element to increase the sensitivity of the antenna array. The Arduino board performs analog-to-digital conversion of the detector output voltages using the on-board ADC. Finally, MATLAB code is used for post-processing the data and generating the source image.

4.2. ELECTRONIC COMPONENTS OF THE SENSOR

This section elaborates on three components that serve as a supplement to the previous section. Figure 4.3 depicts a multiplexer breakout board from SparkFun, with a model number of 74HC4051. This board allows access to all pins and features of the 74HC4051, which is an 8-channel analog multiplexer.

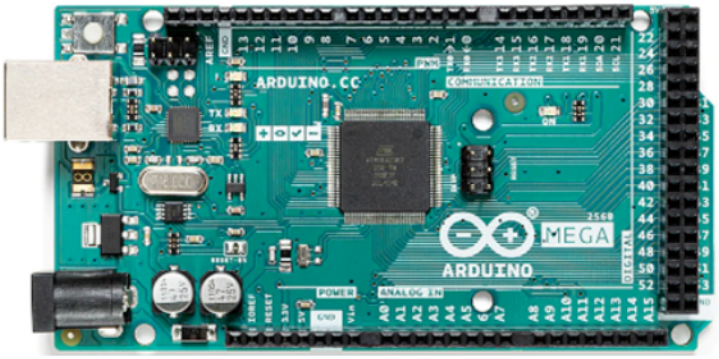

Figure 4.4. Arduino Mega 2560

Figure 4.4 depicts an Arduino Mega 2560 that is utilized for managing multiplexers to scan the antenna components and read the voltage of each element from analog output. The voltage value is transmitted via a serial port. The microcontroller incorporates an ATmega2560 chip that features an 8-bit AVR RISC-based architecture with 256 KB ISP flash memory and a 16-channel 10-bit A/D converter.

Figure 4.5 exhibits an instrumentation amplifier module, specifically the AD 620 from Proto, which amplifies the small DC signal produced by the detector board before it is read by Arduino board. This serves to increase the sensitivity of the camera sensor. However, it is worth noting that the noise originating from the multiplexer is also amplified. Therefore, identifying an appropriate approach to mitigate the noise is crucial for future work.

4.3. CHARACTERIZATION OF THE ANTENNA ARRAY (NO AMPLIFIER)

Figure 4.6 displays the measurement setup utilized for characterizing the antenna array.

An Arduino board is employed to read the output voltage from the antenna array, while the distance between the array and horn antenna is fixed at 15 cm. The distance between the two antennas remains constant, and the RF generator's output power is varied.

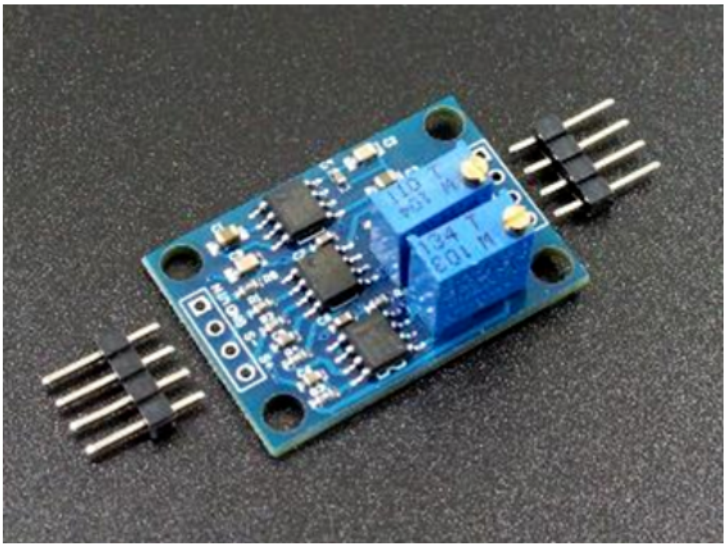

Figure 4.5. Proto Amplifier Module AD 620

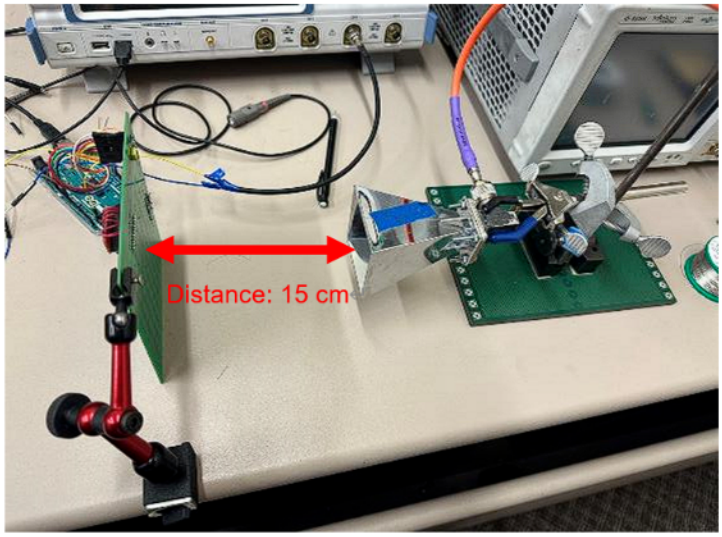

Figure 4.6. Measurement Setup for Antenna Array

Figure 4.7 depicts the the maximum voltage of an antenna array (across all elements) as

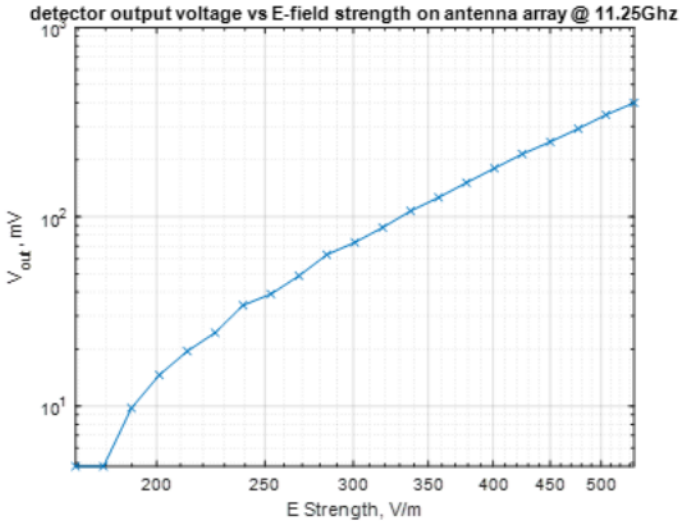

Figure 4.7. Maximum Voltage of Antenna Array vs E Field Strength

the function of the electric field amplitude. As the E-field strength increases, the detector's output voltage also increases, eventually reaching the detector board's output limit. An example image produced by the sensor is presented in Figure 4.8.

Figure 4.8 shows the output voltage of the detector element in antenna array. The output voltage is represented by a color scale. As the voltage magnitude increases, the color intensity deepens, indicating a higher voltage level. This color mapping scheme serves as a useful tool for visualizing and interpreting the pattern of unknown EMI source .The array's output is directly linked to the Arduino ADC, without the use of an amplifier. Given a 5V reference, the 10-bit ADC can detect a minimum measurable voltage of 4.9 mV.

4.4. ACHIEVABLE SENSITIVITY WITH THE AMPPLIFIER

In order to enhance the sensitivity of the array sensor, an instrumentation amplifier board has been inserted between the antenna array and the Arduino board. As a result, the minimum detectable power of the antenna array has improved. However, the sensitivity of the system is now restricted by the multiplexer switching noise.

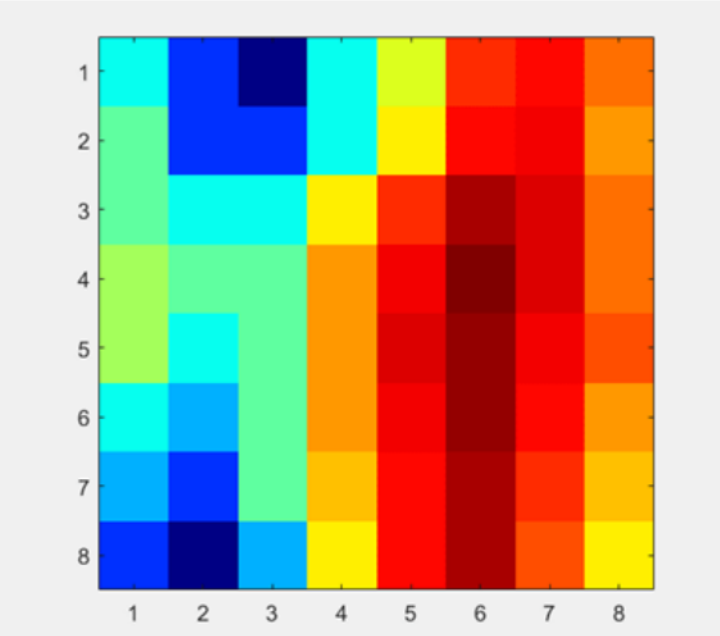

Figure 4.8. Image Produced by The Sensor in The Setup in Figure 4.6

4.5. FRAME RATE

The frame rate is a measure of the number of frames captured by the camera sensor in one second, indicating the speed at which it can detect EMI sources. Figure 4.10 illustrates the measurement setup(no amplifier is used). The output voltage of the camera sensor is recorded by an oscilloscope, as demonstrated in Figure 4.11. The period of the output signal is 84 ms, resulting in a frame rate of approximately 12 Hz.

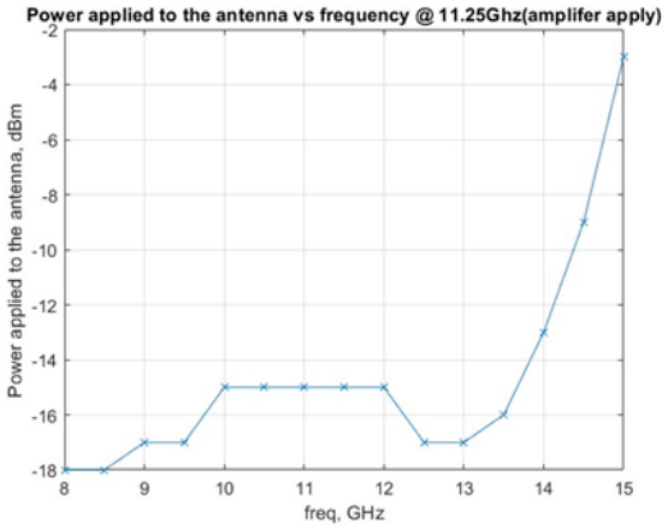

Figure 4.9. The Sensitivity of Camera Sensor with The Amplifer

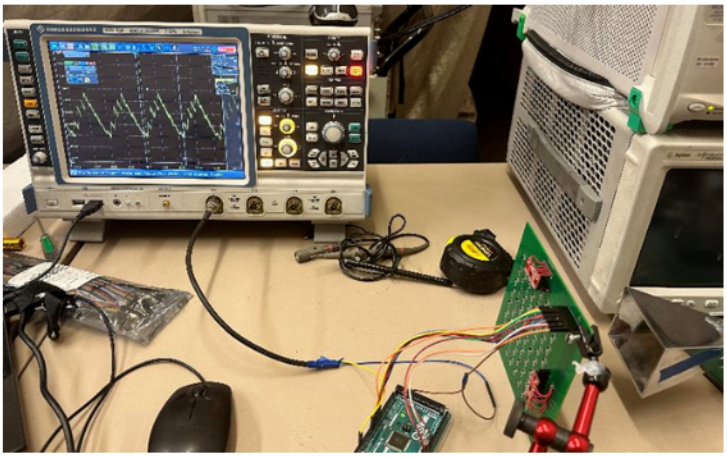

Figure 4.10. Frame Rate Measurement Setup

Figure 4.11. Camera Sensor Output Voltage Waveform

5. CONCLUSIONS

This paper proposes and prototypes a real-time microwave camera sensor, and characterizes its sensitivity and frequency response. Specifically, it describes the design and implementation of a real-time microwave camera that uses a zero-bias diode detector array. The author begins by comparing our approach with previous work, highlighting its cost-effectiveness and simplicity, and noting that it can provide EMI imaging in seconds.

Two prototypes are created to evaluate the performance of the camera sensor. One prototype is a slot antenna, which is characterized using CST and measurement techniques. The other prototype is the detector circuit. Multiple measurements are performed to evaluate the sensitivity of the detector board and the gain of the slot antenna. Finally, the two boards are combined to evaluate the overall performance, and the results are used for further antenna array design.

The author characterizes the antenna array and describe the architecture of the camera sensor, including information about its electric components. The author evaluates the achievable sensitivity of the camera with and without an amplifier, and measure the frame rate to demonstrate the speed of the camera's imaging updates.

Overall, this paper presents a novel approach to real-time microwave imaging using a zero-bias diode detector array. The results demonstrate the potential applications of the camera sensor in EMI source imaging.

REFERENCES

[1] P. Maheshwari, H. Kajbaf, V. Khilkevich, and D. Pommerenke. Emission source microscopy technique for emi source localization. *IEEE Transactions on Electromagnetic Compatibility*, 58(3):729–737, 2016.

[2] M. T. Ghasr Balanis, M. A. Abou-Khousa, S. Kharkovsky, R. Zoughi, and D. Pommerenke. Portable real-time microwave camera at 24 ghz. *IEEE Transactions on Antennas and Propagation*, 60(2):1114–1125, FEb.2012.

[3] C. A. Balanis. *Antenna theory: Analysis and design*. Wiley Blackwell, 2016.

[4] Rf and microwave power detection with schottky diodes - infineon. `https://www.infineon.com/dgdl/Infineon-AN_1807_PL32_1808_132434_RF%20and%20microwave%20power%20detection%20-AN-v01_00-EN.pdf?fileId=5546d46265f064ff0166440727be1055`. Accessed: 2023-02-18.

VITA

In 2018, Liang Liu obtained his B.E degree from Xidian University in Xi'an, Shaanxi, China. He became a member of the Electromagnetic Compatibility Laboratory (EMC lab) in 2020, where he conducts research in signal integrity, dielectric material characterization, and EMI source imaging. Liang received master degree from Missouri University of Science and Technology in May 2023.